ACS OMEGA

Open Access

http://pubs.acs.org/journal/acsodf

Article

Ab Initio Investigation of the Structural, Elastic, Dynamic, Electronic, and Magnetic Properties of Cubic Perovskite $CeCrO_3$

Omer Kabi, Mohammed S. Abu-Jafar,* Mahmoud Farout,* Ahmad A. Mousa, Abdelmadjid Bouhemadou, Nazia Erum, Said M. Azar, Ahmed Bassalat, Hadil Abualrob, Ahmad Y. Thabaineh, and Rabah Khenata

Cite This: *ACS Omega* 2024, 9, 11820−11828

Read Online

ACCESS | Metrics & More | Article Recommendations

ABSTRACT: We presented the results of various aspects related to structural, elastic, electronic, dynamic, and magnetic parameters of cubic perovskite $CeCrO_3$ by means of the full-potential linearized augmented plane wave (FP-LAPW) approach. The calculation of the unit cell volume against the total energy curve confirms that $CeCrO_3$ exhibits higher energetic stability in the ferromagnetic (FM) order. Calculated structural aspects at equilibrium demonstrate excellent similarity to present information, lending credibility to our results. Moreover, monocrystalline elastic constants have been analyzed numerically. These constants provide insights into several related properties, including elastic anisotropy, mechanical stability, and several polycrystalline elastic aspects. Furthermore, the phonon dispersion curves obtained from our calculations reveal the existence of soft modes, which suggests the potential metastability of $CeCrO_3$. Through an analysis of the energy band dispersions, the half-metallic nature of this material is confirmed, such as E_g = 3.00 and 3.13 eV for the HM state within generalized gradient approximations Perdew−Burke−Ernzerhof (GGA-PBE) and Tran−Blaha modified Becke−Johnson (TB-mBJ) calculations, respectively, as well as the FM total magnetic moment of 4.000 μB. Partial density of states (PDOS) aided in identifying the electronic states that contribute to the energy bands. Finally, the computed total magnetic moment aligns fit the theoretical findings available in the literature.

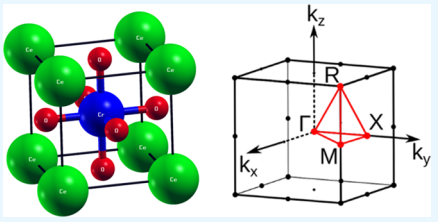

1. INTRODUCTION

Perovskite materials exhibit remarkable tunability in terms of their chemical composition, electronic and magnetic properties, and optical characteristics. This has led to extensive study of the electromagnetic aspects of rare-earth (RE) and transition metal-based perovskites, such as $RECrO_3$, due to their diverse range of applications and the complexity of their structures and physical properties.[1−3] In general, $RECrO_3$ compounds adopt the perovskite structure (space group $Pm\bar{3}m$ (no. 221)), which is cubic in nature. In this crystal structure, the rare earth (RE) atom is located at the (0, 0, 0) site, the chromium (Cr) atom is situated at the (1/2, 1/2, 1/2) position, while face-centered locations at (1/2, 1/2, 0), (0, 1/2, 1/2), and (1/2, 0, 1/2) are occupied by oxygen atoms.

Rare-earth and transition metal-based perovskites remain the focus of various theoretical as well as experimental inquiries.[4−9] Shukla et al. conducted a study on $CeCrO_3$ nanocrystals, where they synthesized and investigated their properties. They observed that $CeCrO_3$ exhibits antiferromagnetic behavior and possesses an optical gap in the visible-light range.[4] In $CeCrO_3$, the magnetic moments of Ce^{3+} and Cr^{3+} are antiparallel, resulting in magnetization compensation.[2] Furthermore, the spin-flip phenomenon evoked by the Zeeman energy concerning entire magnetic moments is responsible for the reversal of external magnetic field magnetization in $CeCrO_3$. Additionally, optical transitions in oxygen p states and transition metal d-states have a major influence on the electronic parameters of Ba(Zr, Hf)O_3 perovskites.[5] Rashid et al. inspected structural, magnetic, and electronic aspects of perovskite $CeCrO_3$.[6] Their conclusion suggests that the compound exhibits a half-metallic ferromagnetic nature with a total magnetic moment of 4 μ_B. Recently, the $DyFeO_3$ compound[7] has been investigated as being multiferric and ferroelectric in nature. Perovskite oxides (ABO_3), which are frequently found in the rare-earth transition-metal oxides of the RMO_3 (R = La, Lu; M = Ti, Cr, Mn, Fe) formula, are the subject of this study in situ high-pressure X-ray diffraction.[8] In addition to this, the FP-LAPW method is employed by Shawahni et al. to study the structural, mechanical, and optoelectronic parameters of $SrTMO_3$ (TM = Rh, Zr) compounds.[9]

The inspiration for the exploration of the $CeCrO_3$ compound is its possible utility in spintronics, magnetic

Received: November 25, 2023
Revised: February 9, 2024
Accepted: February 13, 2024
Published: February 27, 2024

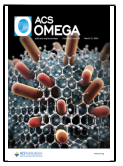

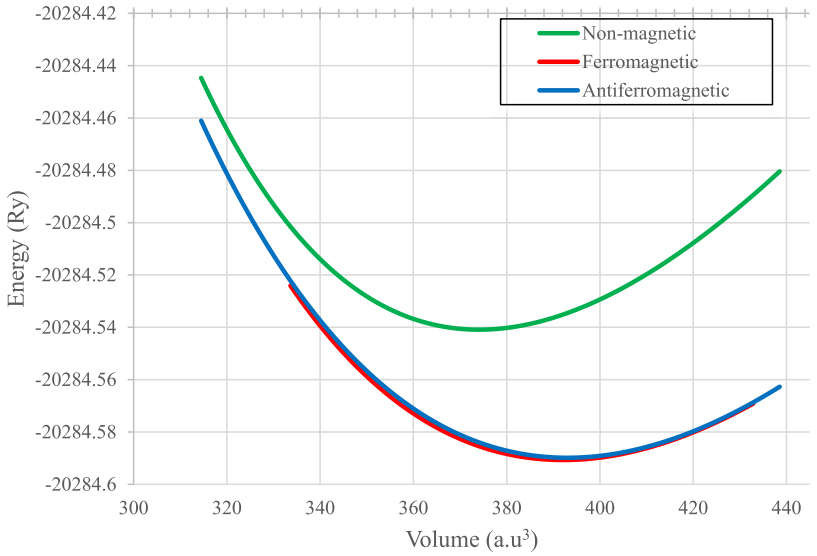

Figure 1. Total energy as a function of volume for the cubic perovskite of $CeCrO_3$ for NM, FM, and AFM phases.

switching devices, and various related fields. This article covers the investigation of fundamental aspects of $CeCrO_3$ compounds. Although theoretical and experimental research on these compounds is rare, it is necessary to establish aspects of the material. To cover this lack of work, we utilized density functional theory (DFT) to find out the structural, elastic, electronic, dynamic, and magnetic aspects of perovskite $CeCrO_3$. No study was found that calculated the dynamical and mechanical aspects. Therefore, to fulfill this absence of work, we calculate these properties. The paper is organized into the following sections. The calculation method is discussed in Section 2. Section 3 presents the most significant results obtained. Finally, the last part provides the deduction summarizing focused findings.

2. COMPUTATIONAL METHOD

In this investigation, to solve the one-electron Kohn−Sham equations state-of-the-art density functional theory (DFT), the FP-LAPW method is implemented in WIEN2k package,[10−12] which is used to calculate the structural and electronic parameters of the cubic perovskite $CeCrO_3$. To model exchange-correlation functionals, Perdew−Burke−Ernzerhof generalized gradient approximation (PBE-GGA) functional[13] is employed to cover structural and mechanical properties. Additionally, to examine the electronic structure, the Tran−Blaha modified Becke−Johnson (TB-mBJ) potential[14] is employed. To enhance the accuracy of electronic structure calculations, the TB-mBJ functional was developed specifically for solids, particularly for obtaining more reliable band gap estimates in semiconductors and insulators. In the FP-LAPW approach, the unit cell is separated into two individual regions. The first region, known as the muffin-tin spheres space, comprises spheres with radii R_{MT} surrounding the atoms. These spheres are designed to encompass all core electrons without overlapping. The second region, termed the interstitial region, corresponds to the space between the muffin-tin spheres. Within the spheres of muffin-tin, the electronic wave functions are extended using a spherical harmonic basis with a maximum orbital angular momentum (l_{max}) restriction. On the other hand, in the interstitial region, the wave functions are expanded using a plane-wave basis, with the largest reciprocal lattice vector (K_{max}) that is used to find the cutoff. To ensure accurate calculations of the total energy, a cutoff parameter $l_{max} = 10$ has been chosen for the spherical harmonics basis set, and a reciprocal lattice vector cutoff $K_{max} = 8/R_{MT}^{min}$ is determined based on the size of the smallest muffin-tin sphere R_{MT}^{min}. The Ce atom is located at (0, 0, 0), the Cr atom at (1/2, 1/2, 1/2), and the oxygen atoms sit at face-centered positions (1/2, 1/2, 0), (0, 1/2, 1/2), and (1/2, 0, 1/2).

Furthermore, the muffin-tin sphere radii for Ce, Cr, and O are specified as 2.50, 1.83, and 1.66 Bohr, respectively. The total energy remains stably self-consistent with a convergence criterion of 10^{-5} Ry. To ensure sufficient accuracy for total energy self-consistent calculations, a special 12 × 12 × 12 Monkhorst−Pack[15] k-point mesh is employed to sample the Brillouin zone (BZ).

3. RESULTS AND DISCUSSION

3.1. Structural Properties. Structural optimization by minimizing the total energy of $CeCrO_3$ with respect to varying unit cell volume was performed for ferromagnetic, nonmagnetic, and antiferromagnetic phases to obtain the equilibrium lattice parameter (a_o), bulk modulus (B), pressure derivative of the bulk modulus (B'), and ground state energy (E_0) corresponding to equilibrium volume V_0. The obtained total energy (E) of $CeCrO_3$ as a function of volume (V) was fitted using the equation of state (EOS)[16]

$$E(V) = E_0 + \frac{VB}{B'}\left\{\left[\left(\frac{V_0}{V}\right)^{B'}/(B'-1)\right] + 1\right\} - \left[\frac{BV_0}{B'-1}\right] \quad (1)$$

Using the calculated total energies, it was possible to compare the relative stability of various magnetic phases, ferromagnetic (FM), antiferromagnetic (AFM), and nonmagnetic (NM) configurations. Figure 1 shows the energy−voltage diagram of $CeCrO_3$ for different magnetic phases. The energies of the AFM and NM phases lie higher than that of the FM phase.

The relative stabilities of several magnetic phases, FM, AFM, and NM configurations, are compared using the computed total energies. The energy−volume diagram of $CeCrO_3$ for various magnetic phases is displayed in Figure 1. The NM and

https://doi.org/10.1021/acsomega.3c09292
ACS Omega 2024, 9, 11820−11828

AFM phases have energies that are higher than those of the FM phase.

The most stable configuration is the FM phase, which has the lowest minimum energy in the energy−volume curve. We calculated the lattice parameter a_0 using the value V_0, which corresponds to the lowest minimum energy, as systems always try to reduce their energy. The value was found to be 3.877 Å, which is compatible with the previous study (3.877 Å).[6] The total energy, lattice parameter, bulk module, and its derivative with respect to the pressure for the different phases are listed in Table 1.

Table 1. Calculated Equilibrium Lattice Parameter (a_0), Bulk Modulus (B), and Pressure Derivative of B (B') and Ground State Energy (E_0) of $CeCrO_3$ for Different Phases

magnetic phase	a_0 (Å)	B (GPa)	B'	E_0 (Ry)
FM	3.877	182.234	4.308	−20284.590710
AFM	3.8763	175.9224	3.1571	−20284.585351
NM	3.813	213.018	4.600	−20284.540896
others[6]	3.877	183.810		

The stability of the structures in the cubic phase was verified using the tolerance factor. The calculation of the tolerance factor was done by using the relation $t = \frac{0.707(r_{Ce} + r_o)}{r_{Cr} + r_o}$. Here, $r_{Cr} + r_o$ characterizes the difference between Cr and O atoms, while it authenticates from calculations that $CeCrO_3$ possesses a 0.95−0.99 value of tolerance factor.

Figure 1 and Table 1 show that the FM is the ground state energy, so we have excluded the NM and AFM phases and proceeded with the FM phase.

3.2. Elastic Properties. We employed the Morteza package,[17] developed and integrated into the WIEN2k code, to determine the monocrystalline elastic constants (C_{ij}) for the cubic crystal structure of $CeCrO_3$. This method utilizes the total energy versus strain relationship to determine the C_{ij} values. The theoretical details of this method can be found in the referenced work of Morteza.[17] In Table 2, the obtained C_{ij} values are presented. It can be followed that the C_{ij} calculated values satisfy cubic crystal standard Born's stability criteria[18] ($C_{11} > 0$, $C_{11} + 2C_{12} > 0$, $C_{11}-C_{12} > 0$, and $C_{44} > 0$), indicating the mechanical stability of $CeCrO_3$. In practical applications, synthesized materials are often polycrystalline aggregates. Therefore, it becomes necessary to determine their isotropic elastic moduli, namely, the isotropic Young's modulus (Y), bulk modulus (B), Poisson's ratio (ν), and shear modulus (G). The Voigt−Reuss−Hill (VRH) approximations[19−21] can be employed to estimate these elastic moduli from the monocrystalline elastic constants. As per the VRH methodology, the modulus for polycrystals can be achieved by taking the arithmetic mean of Voigt and Reuss bounds in lieu of nanocrystals. Specifically, shear modulus G for a cubic crystal can be evaluated by using the subsequent criteria

$$G_R = 5(C_{11} - C_{12})C_{44}/[4C_{44} + 3(C_{11} - C_{12})] \quad (2)$$

$$G_V = \frac{1}{5}(C_{11} - C_{12} + 3C_{44}) \quad (3)$$

The terms "V" and "R" in the equations imply Voigt's and Reuss's approximations, respectively. For bulk modulus, the Voigt and Reuss approximations yield the same relationship

$$B = \frac{1}{3}(C_{11} + 2C_{12}) \quad (4)$$

By utilizing the considered B and G terms, one can further determine Young's modulus Y and Poisson's ratio ν, commonly estimated for polycrystalline compounds for assessing the hardness using the following equations

$$Y = \frac{9BG}{(G + 3B)};\ \nu = \frac{3B - 2G}{2(3B + G)} \quad (5)$$

The values for the polycrystalline elastic moduli are presented in Table 2. They highlight that $CeCrO_3$ has a medium strength. These elastic moduli provide valuable insights into various physical phenomena exhibited by the material. Pugh's ratio B/G larger than 1.75 categorizes the material as ductile, whereas a ratio below 1.75 indicates brittle behavior.[22] Based on our calculations, the B/S ratio of $CeCrO_3$ is determined to be 2.46, classifying it as a ductile material. Furthermore, Poisson's ratio can offer evidence about the nature of bonding forces and the material's stability. A Poisson's ratio greater than 0.25 suggests predominantly ionic bonding in the compound, whereas a value below 0.25 indicates predominantly covalent bonding. In the case of $CeCrO_3$, the calculated Poisson's ratio is 0.321, indicating a predominantly ionic nature of the chemical bonds in the compound.

The characterization of elastic anisotropy in crystals holds significant importance due to its association with various physical phenomena in materials.[23] In this study, we employed anisotropy factor A as a metric to quantify the degree of elastic anisotropy. In an isotropic crystal, the A value equals unity, thereby serving as a baseline. Consequently, deviation of A from unity confers the extent of elastic anisotropy present in the material under consideration.[24] For $CeCrO_3$, we calculated the value of A to be 0.194, suggesting a pronounced elastic anisotropy within the material. This value highlights a substantial departure from isotropy, indicating significant variations in the elastic properties along different crystallographic directions.

3.3. Elastic Anisotropy. The anisotropy of physical properties in crystals arises from the varying bonding characteristics along different crystal directions. Elastic anisotropy plays a crucial role in influencing various properties of crystals, including phase changes, internal friction, unique phonon modes, and crack behavior.[25−28] Therefore, it is used to quantify the degree of elastic anisotropy in crystals to predict its effects on associated physical processes. Three-dimensional (3D) and two-dimensional (2D) representations serve as effective tools for visualizing this directional dependence. In the case of the isotropic elastic modulus, a

Table 2. Calculated Monocrystalline Elastic Constants (C_{ij}, in GPa), Polycrystalline Moduli, Including the Bulk Modulus (B, in GPa), Shear Modulus (G, in GPa), Young's Modulus (Y, in GPa), Poisson's Coefficient (ν, Dimensionless), Pugh Coefficient (B/G, Dimensionless), and Anisotropy Factor (A, Dimensionless) of $CeCrO_3$ in the Cubic Structure

C_{11}	C_{12}	C_{44}	B	G	B/G	Y	ν	A
357.9	83.0	26.7	174.6	71.0	2.459	187.6	0.321	0.194

https://doi.org/10.1021/acsomega.3c09292
ACS Omega 2024, 9, 11820−11828

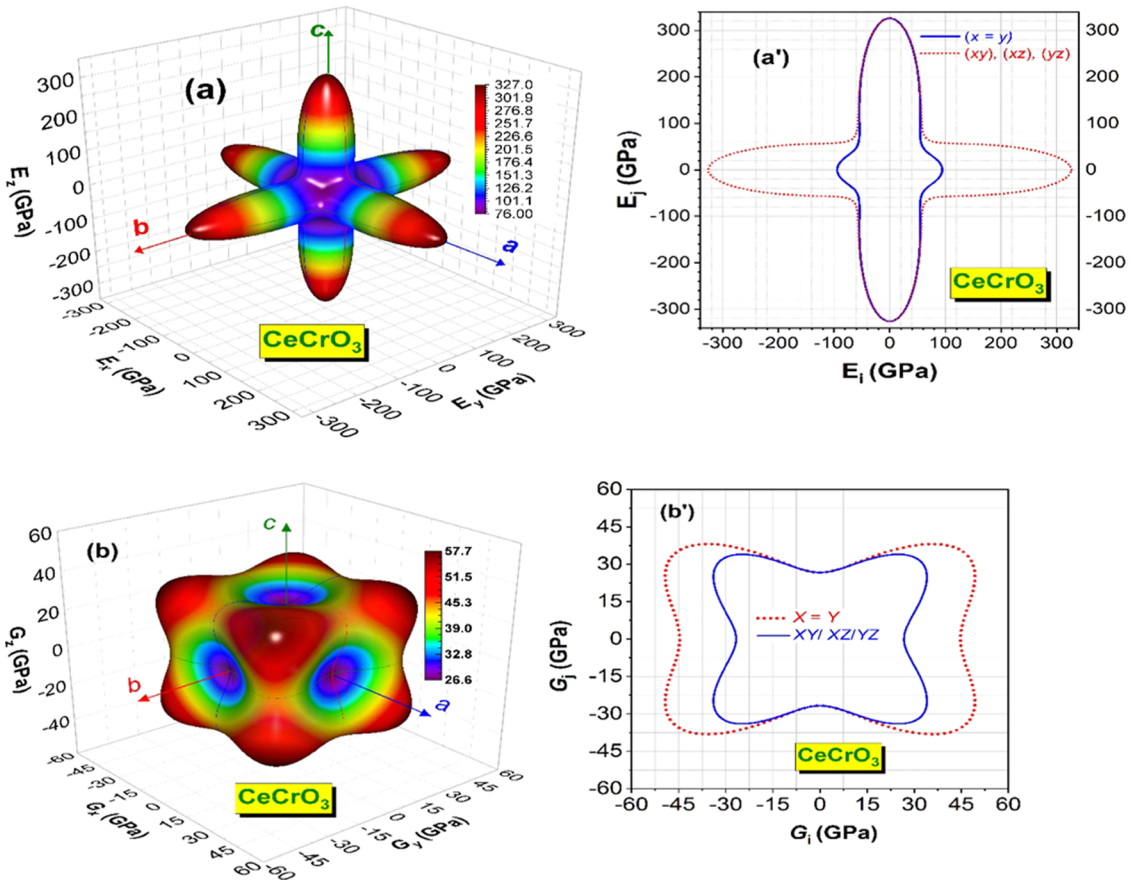

Figure 2. Calculated three-dimensional representations (stereograms) of Young's modulus (E) (panel (a)) and shear modulus (G) (panel (b)) for the $CeCrO_3$ cubic perovskite. Additionally, the cross sections of the stereograms in the $x = y$ and $xy/xz/yz$ planes are represented (panels (a′) and (b′)).

perfectly spherical closed 3D surface and a circular form curve in the 2D representation depict the crystal direction dependence of the modulus. Consequently, any deviation from the spherical shape in the 3D representation or from the circular form in the 2D representation indicates the level of anisotropy exhibited by the elastic modulus being analyzed. Y and G in a cubic crystal are mathematically described as[29,30]

$$Y(\theta, \varphi) = (S_{11} - 2SJ)^{-1};\ G(\theta, \varphi) = (S_{44} + 4SJ)^{-1} \quad (6)$$

Here, $S = S_{11} - S_{22} - 0.5S_{44}$ and $J = \sin^2\theta\cdot\cos^2\theta + 0.125\sin^4\theta(1 - \cos 4\varphi)$. In this context, θ and φ are the Euler angles, and S_{ij} are the elastic compliance constants. Figure 2 depicts both three-dimensional (3D) and two-dimensional (2D) representations of Young's modulus and shear modulus for $CeCrO_3$. Additionally, their cross sections in the xy, xz, and $x = y$ planes exhibit significant deviations from circular shapes. These observations indicate a pronounced anisotropy in the elastic moduli E and G, thereby signifying a substantial elastic anisotropy in $CeCrO_3$. The maximum value of Young's modulus (E_{max}) is observed along the <100> direction, with a magnitude of 327.0 GPa. Conversely, the corresponding minimum value (E_{min}) is observed along the <111> direction, measuring 76.0 GPa. Furthermore, the maximum value of the shear modulus (G_{max}) is observed along the <111> direction, amounting to 57.7 GPa. In contrast, the minimum value (G_{min}) is observed along the <100> direction, measuring 26.6 GPa. These substantial discrepancies between the maximum and minimum values of Young's modulus and shear modulus underscore significant elastic anisotropy exhibited by $CeCrO_3$.

3.4. Electronic Properties. *3.4.1. Band Structure.* Any material's electronic properties, such as its energy band gap and density of states (TDOS and PDOS), are crucial to understanding its electronic behavior. The band structure of any given material can be used to determine whether or not it is appropriate for a given role.

This section is devoted to calculating the band diagrams for the spin down and up for the $CeCrO_3$ alongside the Brillouin zone at zero pressure, in high symmetry directions have been depicted in Figure 3a,b and in Table 3, respectively.

Table 3 shows the comparison between results using approximation PBE-GGA and then by utilizing the mBJ potential. It can be observed from Table 3 that both correlation results are in good accordance with each other, revealing the metallic and indirect nature of the band gap of about 3 eV. The detailed discussion of separate channels implies that in down spin channels, the valence band maximum (VBM) ensues at the M-symmetry point; however, a conduction band minimum (CBM) occurs along the Γ-point along with an energy gap of about 3 eV.

The calculations of the energy band gap have been improved by a modified Beke−Johnson potential (mBJ-GGA). As shown in Figure 4a,b, in the case of spin up, the band gap remains metallic. However, in the spin-down channel, a very small percentage of energy gap was observed to be about 3.13 eV. That means that the material is a semiconductor in this

https://doi.org/10.1021/acsomega.3c09292
ACS Omega 2024, 9, 11820−11828

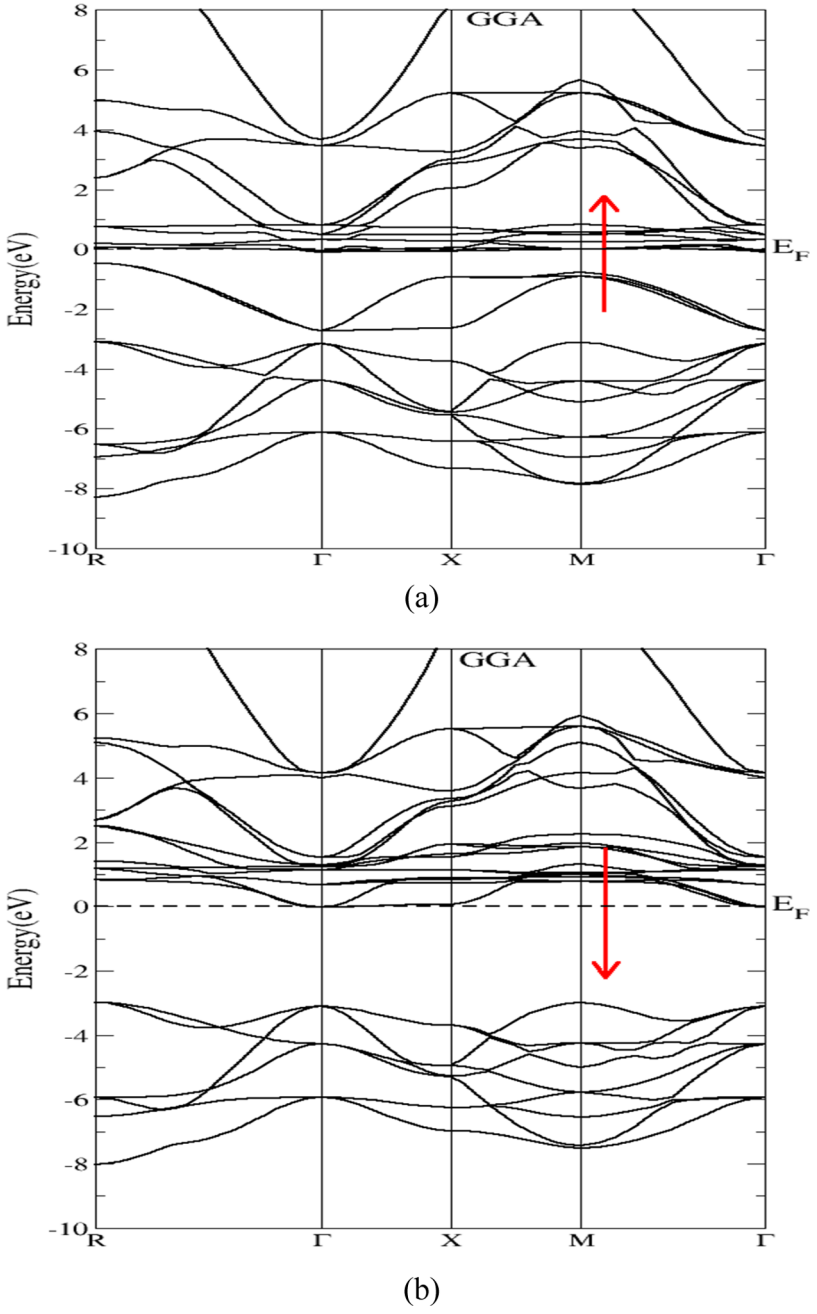

Figure 3. Calculated spin-polarized (a) up and (b) down band structures for a cubic $CeCrO_3$ compound using PBE-GGA.

Table 3. Energy Band Gap (E_g) in eV of $CeCrO_3$ Compound Using PBE-GGA and mBJ-GGA Methods

materials	structure	spin	band gap type	E_g-GGA	E_g-mBJ-GGA	other theoretical results
$CeCrO_3$	cubic	up	···	metallic	metallic	
		down	indirect	M → Γ 3 eV	M → X 3.13 eV	2.89 eV[6]

channel, as figured in Figure 4b. The calculated band gap within the mBJ-GGA has been recorded by Rashid et al.,[6] who obtained a value of 2.89 eV, which is in exact alliance with our values. No significant spin−orbit interaction was found because the interaction provided by the spin−orbit has no effect on the electronic aspects of our compound.

There are primarily two types of exchanges that lead to band gaps in solids: d-d hybridization and charge transfer. In line with other perovskites, our compound's charge transfer gap is the most dominant of these.

3.4.2. Density of States. In this section, at each energy occupied description of the ratio of states has been illustrated as shown in Figures 5 and 6. Here for cubic $CeCrO_3$, the density of states (DOS) (total and partial) are evaluated by using PBE-GGA. In Figures 5 and 6, spin-up and spin-down densities are compared with respect to each other. The contribution of states is as follows: the valence band contribution for the spin-up states comes majorly from the Cr-d states in addition to a minute involvement of the p-state of oxygen, whereas the origin of the conduction band comes

https://doi.org/10.1021/acsomega.3c09292
ACS Omega 2024, 9, 11820−11828

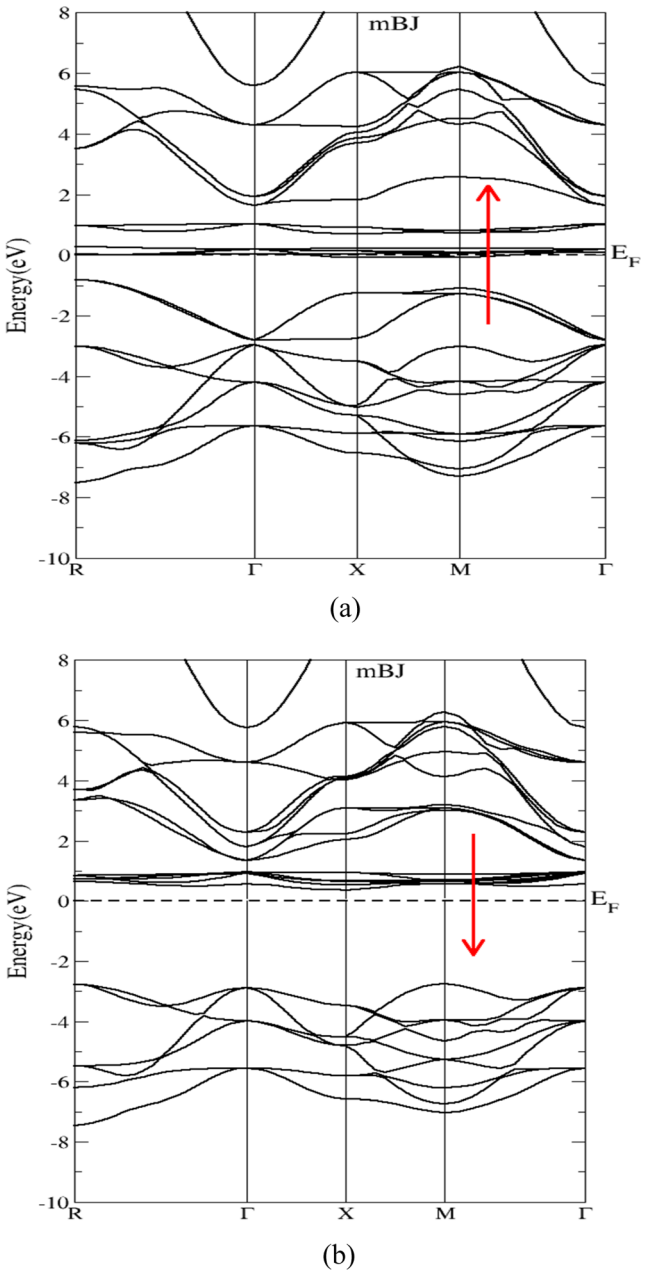

Figure 4. Calculated spin-polarized (a) up (b) down band structures for the cubic $CeCrO_3$ compound with the mBJ-GGA potential.

from f-states of Ce with little contribution from d-states of chromium and further contribution is from the Ce-f and Cr-d states. Next, the valence band contribution for the spin-down states comes via the O-p states of chromium, along with a little contribution from the Cr-d states. It is obvious that the spin-up state in Figures 5a and 6a is metallic, while the spin-down state is semiconducting, which confirms that the compound $CeCrO_3$ is a half-metal.

Strong hybridization by Ce-p and Ce-d and minor effects from the O-s and the O-p states are visible in the uppermost portion of the valence band region. Sigma bonding combinations of the sigma type between the d orbitals of Ce-d and Cr-d states provide a good way to take advantage of this phenomenon. After that, Ce-d, Ce-f, and Cr-d orbitals are the primary sources of state contributions in the conduction band region. Thus, it is evident that there is strong hybridization between the Cr-3d and the O-2p orbitals, confirming the ionic character.

3.5. Magnetic Properties. In this subsection, we elaborate on the magnetic behavior of the compound of interest in terms of the magnetic property. In the first place, we calculate the magnetic moments for the studied compound, which is further compared with the available results as tabulated in Table 4. From these results, it is obvious that this compound is ferromagnetic. The main contribution comes from both the Cr and Ce atoms. The total magnetic moment is ~4 μ_B, which is in good agreement with other theoretical results.[6]

The main contribution of the total magnetic moment comes from the contribution of the magnetic moment of Cr and Ce atoms. The total magnetic moment is found to be ~4 μ_B, which is in good agreement with other theoretical results.[6] Therefore, the d-states of Cr, which are in the spin-up channel close to the Fermi level, are the primary source of the magnetic moment. The large exchange splitting of the Cr-3d states into the t_{2g} and e_{2g} states is what produces the chromium moment. We can better understand the magnetism of this perovskite by looking at its DOS because there is a strong correlation between its electronic structure and magnetic properties. In fact, this chromium atom split is seen in the DOS spectra; for instance, in the spin up, we observe the presence of the t_{2g}. This indicates that while states e_{2g} are empty, states t_{2g} are partially filled. On the other hand, in the spin down, they are visible in the conduction band region rather than the valence band region, indicating that Cr-d e_{2g} and Cr-d t_{2g} are entirely empty in this channel. This can also be explained by the perovskite's crystalline structure, which is depicted in Figure 1. As a result, the chromium atom's magnetic moment increases due to an increase in exchange splitting between the e_{2g} and t_{2g} states.

3.6. Dynamic Properties. To assess the stability of $CeCrO_3$ dynamically, we employed a finite displacement approach inside density functional perturbation theory (DFPT) using the CASTEP code.[31] It uses the pseudopotential plane-wave method. For overall energy accurate predictions, a cutoff of 850 eV is utilized for the plane-wave basis set and a 10 × 10 × 10 Monkhorst−Pack scheme *k*-point grid for Brillouin zone (BZ) evaluation was utilized. By employing the aforementioned methodology, we obtained the phonon dispersion diagram, which is depicted in Figure 7. In the study of materials, the absence of the soft mode in the phonon dispersion curve indicates dynamic stability.[32] Consequently, the presence of soft modes, manifested as phonon dispersion negative frequencies, implies dynamic instability of $CeCrO_3$. Soft modes initiate lattice instability that potentially induces a structural phase transition. Furthermore, the occurrence of soft modes suggests that synthesizing the compound under normal conditions may be challenging.

From the point of view of analysis, the computation of phonon modes suggests that our compound is unstable. However, mechanical stability can be verified from the elastic property calculation of the cubic crystal. It is an overall perception that a metastable state exists if the compound is unstable dynamically but stable mechanically, which is in accordance with our results.

3.7. Formation Energy. The formation enthalpy (ΔH) of the $CeCrO_3$ compound is calculated to confirm its thermodynamic stability.[33] This parameter is determined by applying the formula 7,[34] which is dependent on the energy of

https://doi.org/10.1021/acsomega.3c09292
ACS Omega 2024, 9, 11820−11828

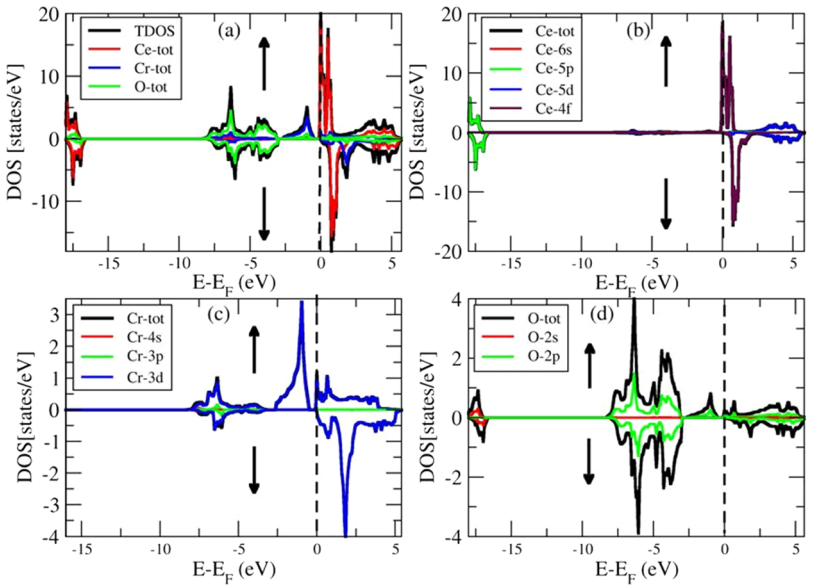

Figure 5. Total and partial density of state of spin up and spin down for (a) total DOS, (b) Ce, (c) Cr, and (d) O of the cubic $CeCrO_3$ compound using the PBE-GGA method.

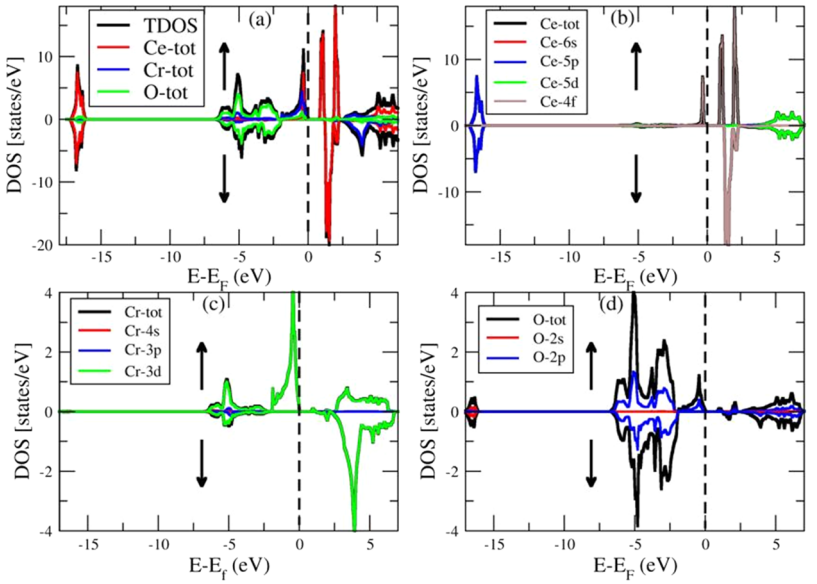

Figure 6. Total and partial density of state of spin up and spin down for (a) total DOS, (b) Ce, (c) Cr, and (d) O of the cubic $CeCrO_3$ compound using the mBJ-GGA method.

Table 4. Total Magnetic Moment for the Cubic $CeCrO_3$ Compound Using PBE-GGA and mBJ-GGA Methods

compounds		magnetic moment (μ_B)				
		Ce	Cr	O_3	interstitial	total magnetic moment (M^{tot}) μ_B
cubic $CeCrO_3$	present (GGA)	1.057	2.331	3 × 0.02807 = 0.084	0.496	3.968
	present (mBJ-GGA)	0.981	2.480	3 × 0.07067 = 0.212	0.327	4.00001
	theoretical result	0.983[6]	2.528[6]	3 × 0.0642[6] = 0.193	0.296	4.000[6]

all of the constituent elements (E^{Ce}, E^{Cr}, and E^{O} for Ce, Cr, and O, respectively) as well as the total energy of $CeCrO_3$ ($E_{tot}^{CeCrO_3}$).

$$\Delta H = E_{tot}^{CeCrO_3} - (E^{Ce} + E^{Cr} + 3E^{O}) \quad (7)$$

The enthalpy shift that occurs when one mole of a material is created from its constituent elements is known as the formation enthalpy of a substance from a thermal standpoint. While producing a substance exothermically, the formation enthalpy can be negative; however, while producing an endothermic substance, the formation enthalpy can be positive.[35] The $CeCrO_3$ compound's formation enthalpy values are negative (−29.3 and −18.2 meV for the ferromagnetic state and the nonmagnetic state, respectively), indicating that both their thermodynamic stability and the exothermic nature of their interaction are confirmed. Also, the negative formation

https://doi.org/10.1021/acsomega.3c09292
ACS Omega 2024, 9, 11820−11828

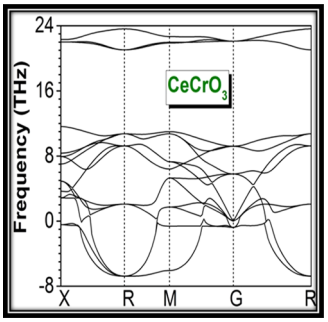

Figure 7. Calculated phonon dispersion curve along the high symmetry lines in the Brillouin zone for $CeCrO_3$.

energies indicate the stability of both states (but the ferromagnetic state is more stable than the nonmagnetic state); thus, they could be synthesized in the laboratory using appropriate techniques.

4. CONCLUSIONS

In this study, a comprehensive investigation of cubic $CeCrO_3$ is performed to explore its structural, electronic, elastic, and magnetic properties. To accomplish this, we employed the method of FP-LAPW using DFT. For generalized gradient approximations, Perdew–Burke–Ernzerhof (GGA-PBE) exchange-correlation energy is used for the calculations of structural and elastic properties. In addition to GGA-PBE, the TB-mBJ potential is utilized for the calculation of electromagnetic features. To determine the ground state structural parameters, total energy is fitted with volume of unit and it is concluded that the $CeCrO_3$ compound is stable within ferromagnetic order. The phonon dispersion calculations verify the metastable character of the current compound. The elastic properties and anisotropic aspects reveal the ductile and anisotropic nature of this compound. Furthermore, band structure analysis corresponds to CeCrO3, demonstrating half-metallic characteristics. Subsequent analysis is being expanded by utilizing PDOS plots, which helped to identify the nature of the energy bands. Furthermore, our calculations yield a total magnetic moment of approximately 4 μ_B, aligning with other theoretical results available. Hopefully, this work delivers useful findings of structural, elastic, electronic, and magnetic aspects of cubic $CeCrO_3$ for various technological benefits, especially for spintronics devices.

AUTHOR INFORMATION

Corresponding Authors

Mohammed S. Abu-Jafar − *Department of Physics, An-Najah National University, Nablus 00970, Palestine;* orcid.org/0000-0003-1645-4974; Phone: +970599351502; Email: mabujafar@najah.edu

Mahmoud Farout − *Department of Physics, An-Najah National University, Nablus 00970, Palestine;* Email: m.qaroot@najah.edu

Authors

Omer Kabi − *Department of Physics, An-Najah National University, Nablus 00970, Palestine*

Ahmad A. Mousa − *Middle East University, Amman 11831, Jordan; Applied Science Research Center, Applied Science Private University, Amman 11931, Jordan*

Abdelmadjid Bouhemadou − *Laboratory for Developing New Materials and their Characterizations, Department of Physics, Faculty of Science, Ferhat Abbas University, Setif 19000, Algeria*

Nazia Erum − *Institute of Physics, Bahauddin Zakariya University, Multan 60800, Pakistan*

Said M. Azar − *Department of Physics, Faculty of Science, Zarqa University, Zarqa 13132, Jordan*

Ahmed Bassalat − *Department of Physics, An-Najah National University, Nablus 00970, Palestine*

Hadil Abualrob − *Department of Physics, An-Najah National University, Nablus 00970, Palestine*

Ahmad Y. Thabaineh − *Department of Mathematics, An-Najah National University, Nablus 00970, Palestine*

Rabah Khenata − *Laboratoire de Physique Quantique et de Modélisation Mathématique de la Matière (LPQ3M), Université de Mascara, Mascara 29000, Algeria*

Complete contact information is available at: https://pubs.acs.org/10.1021/acsomega.3c09292

Notes

The authors declare no competing financial interest.

ACKNOWLEDGMENTS

The authors would like to thank their universities for providing the necessary facilities to carry out this research.

REFERENCES

(1) Zhou, J.-S.; Alonso, J. A.; Pomjakushin, V.; Goodenough, J. B.; Ren, Y.; Yan, J.-Q.; Cheng, J.-G. Intrinsic structural distortion and superexchange interaction in the orthorhombic rare-earth perovskites RCrO3. *Phys. Rev. B* **2010**, *81*, No. 214115.

(2) Cao, Y.; Cao, S.; Ren, W.; Feng, Z.; et al. Magnetization switching of rare earth orthochromite CeCrO3. *Appl. Phys. Lett.* **2014**, *104*, No. 232405.

(3) Zhu, Y.; Sun, K.; Wu, S.; Zhou, P.; Fu, Y.; Xia, J.; Li, H.-F. A comprehensive review on the ferroelectric orthochromates: Synthesis, property, and application. *Coord. Chem. Rev.* **2023**, *475*, No. 214873.

(4) Shukla, R.; Bera, A.; Yusuf, S.; Deshpande, S.; Tyagi, A.; Hermes, W.; Eul, M.; Pottgen, R. Multifunctional Nanocrystalline CeCrO3: Antiferromagnetic, Relaxor, and Optical Properties. *J. Phys. Chem. C* **2009**, *113*, 12663–12668.

(5) Azar, S. A.; Al-Zoubi, I.; Mousa, A.; Masharfe, R.; Jaradat, E. Investigation of Electronic, Optical and Thermoelectric Properties of Perovskite BaTMO3 (TM = Zr, Hf): First Principles Calculations. *J. Alloys Compd.* **2021**, *887*, No. 161361.

(6) Rashid, M.; Iqbal, M.; Noor, N. DFT-mBJ study of electronic and magnetic properties of cubic $CeCrO_3$ compound: an ab-initio investigation. *Sci. Inquiry Rev.* **2017**, *1*, 22.

(7) Tokunaga, Y.; Iguchi, S.; Arima, T.; Tokura, Y. Magnetic-Field-Induced Ferroelectric State in $DyFeO_3$. *Phys. Rev. Lett.* **2008**, *101*, No. 097205.

(8) Zhou, J.-S. Structural distortions in rare-earth transition-metal oxide perovskites under high pressure. *Phys. Rev. B* **2020**, *101*, No. 224104.

(9) Shawahni, A.; Abu-Jafar, M.; Jaradat, R.; Ouahrani, T.; Khenata, R.; Mousa, A.; Ilaiwi, K. Structural, Elastic, Electronic and Optical Properties of SrTMO3 (TM = Rh, Zr) Compounds: Insights from FP-LAPW Study. *Materials* **2018**, *11*, 2057.

(10) Blaha, P.; Schwarz, K.; Medsen, G. K. H.; Kvasnicka, D.; Luitz, J. *WIEN2k, An Augmented Plane Wave Plus Local Orbitals Program for Calculating Crystal Properties*; Vienna University Technology: Vienna, Austria, 2001. ISBN 3-9501031-1-2.

(11) Schwarz, K.; Blaha, P. Solid state calculations using WIEN2k. *Comput. Mater. Sci.* **2003**, *28*, 259–273.

https://doi.org/10.1021/acsomega.3c09292
ACS Omega 2024, 9, 11820–11828

(12) Schwarz, K. DFT calculations of solids with LAPW and WIEN2k. *J. Solid State Chem.* **2003**, *176*, 319−328.
(13) Perdew, J. P.; Burke, S.; Ernzerhof, M. Generalized gradient approximation made simple. *Phys. Rev. Lett.* **1996**, *77*, 3865.
(14) Becke, A. D.; Johnson, E. R. A simple effective potential for exchange. *J. Chem. Phys.* **2006**, *124*, No. 221101.
(15) Monkhorst, H. J.; Pack, J. D. Special points for Brillouin-zone integrations. *Phys. Rev. B* **1976**, *13*, 5188.
(16) Murnaghan, F. D. The compressibility of media under extreme pressures. *Proc. Natl. Acad. Sci. U.S.A.* **1944**, *30*, 244.
(17) IRelast Package is Provided by M. Jamal as Part of the Commercial Code WIEN2K, 2014. http://www.wien2k.at/.
(18) Born, M. On the stability of crystal lattices. *Math. Proc. Cambridge Philos. Soc.* **1940**, *36*, 160−172.
(19) Voigt, W. Ueber die Beziehung bwischen den beiden Elasticitä tsconstanten isotroper Körper. *Ann. Phys.* **1889**, *38*, 573−587.
(20) Reuss, A. Berechnung der Fließgrenze von Mischkristallen auf Grund der Plastizitätsbedingung für Einkristalle. *Math. Phys.* **1929**, *9*, 49.
(21) Hill, R. The Elastic Behaviour of a Crystalline Aggregate. *Proc. Phys. Soc. A* **1952**, *65*, 349.
(22) Pettifor, D. G. Theoretical predictions of structure and related properties of intermetallics. *Mater. Sci. Technol.* **1992**, *8*, 345−349.
(23) Zener, C. *Elasticity and Anelasticity of Metals*; University of Chicago Press: Chicago, IL, 1948.
(24) Ravindran, P.; Fast, L.; Korzhavyi, P. A.; Johansson, B.; et al. Density functional theory for calculation of elastic properties of orthorhombic crystals: application to TiSi2. *J. Appl. Phys.* **1998**, *84*, 4891.
(25) Ledbetter, H.; Migliori, A. A general elastic-anisotropy measure. *J. Appl. Phys.* **2006**, *100*, No. 063516.
(26) Kube, C. M. Elastic anisotropy of crystals. *AIP Adv.* **2016**, *6*, No. 095209.
(27) Khireddine, A.; Bouhemadou, A.; Alnujaim, S.; Guechi, N.; Bin-Omran, S.; Al-Douri, Y.; Khenata, R.; Maabed, S.; Kushwaha, A. K. First-principles predictions of the structural, electronic, optical and elastic properties of the Zintl-phases AE_3GaAs_3 (AE = Sr, Ba). *Solid State Sci.* **2021**, *114*, No. 106563.
(28) Lloveras, P.; Castán, T.; Porta, M.; Planes, A.; Saxena, A. Influence of Elastic Anisotropy on Structural Nanoscale Textures. *Phys. Rev. Lett.* **2008**, *100*, No. 165707.
(29) Nye, J. F. *Physical Properties of Crystals*; Oxford University Press: Oxford, 1985.
(30) Luan, X.; Qin, H.; Liu, F.; Dai, Z.; Yi, Y.; Li, Q. The mechanical properties and elastic anisotropies of cubic Ni_3Al from first-principles calculations. *Crystals* **2018**, *8*, 307.
(31) Clark, S. J.; Segall, M. D.; Pickard, C. J.; Hasnip, P. J.; Probert, M. J.; Refson, K.; Payne, M. C. First principles methods using CASTEP. *Z. Kristallogr. - Cryst. Mater.* **2005**, *220*, 567−570.
(32) Suetin, D. V.; Shein, I. R. Electronic structure, mechanical and dynamical stability of hexagonal subcarbides M2C (M = Tc, Ru, Rh, Pd, Re, Os, Ir and Pt): Ab initio calculations. *Phys. Solid State* **2018**, *60*, 213−224.
(33) Alrahamneh, M. J.; Khalifeh, J.; Mousa, A. Ab-initio calculations of the structural, mechanical, electronic, magnetic and thermoelectric properties of Zr_2RhX (X = Ga, In) Heusler alloys. *Phys. B* **2020**, *581*, No. 411941.
(34) Mousa, A. A.; Hamad, B.; Khalifeh, J. Structure, electronic and elastic properties of the NbRu shape memory alloys. *Eur. Phys. J. B* **2009**, *72*, 575−581.
(35) Mousa, A. A.; Al-Qaisi, S.; Abu-Jafar, M.; Al Azar, S.; Jaradat, R.; Khalifeh, J.; Ouahrani, T.; Khenata, R. Ab initio studies of the structural, elastic, electronic and optical properties of the Ni3In intermetallic compound. *Mater. Chem. Phys.* **2020**, *249*, No. 123104.

https://doi.org/10.1021/acsomega.3c09292
ACS Omega 2024, 9, 11820−11828